ORIGINAL PAPER



Prediction of wall stress and oxygen flow in patient-specific abdominal aortic aneurysms: the role of intraluminal thrombus

Alexis Throop¹ · Martina Bukac² · Rana Zakerzadeh¹

Received: 17 March 2022 / Accepted: 13 July 2022 / Published online: 30 July 2022 © The Author(s), under exclusive licence to Springer-Verlag GmbH Germany, part of Springer Nature 2022

Abstract

In this study, the biomechanical role of intraluminal thrombus (ILT) in an abdominal aortic aneurysm (AAA) is investigated. The implications of ILT in AAA are controversial in literature. Previous studies have demonstrated that ILT provides a biomechanical advantage by decreasing wall stress, whereas other studies have associated ILT with inhibiting oxygen transport and inducing aortic wall weakening. Therefore, we sought to explore the connection between ILT, mechanical stresses, and oxygen flow in different geometries of patient-specific aneurysms with varying ILT morphologies. The objective is to investigate the extent to which ILT influences the prediction of aneurysmal wall stresses that are associated with rupture, as well as oxygen concentrations to measure tissue oxygen deprivation. Three patient-specific AAA geometries are considered, and two models, one with ILT and one without ILT, are created for each patient to assess the effect of ILT presence. A fluid–structure interaction approach is used to couple the blood flow, wall deformation, and oxygen mass transport. Results are presented for hemodynamics patterns, wall stress measures, and oxygen metrics within the arterial wall. While ILT is found to reduce wall stress, simulations confirm that ILT decreases oxygen transport within the tissue significantly, leading to wall hypoxia.

Keywords Abdominal aortic aneurysm $(AAA) \cdot Intraluminal thrombus (ILT) \cdot Patient-specific \cdot Hypoxia \cdot Arterial wall stress \cdot Fluid \cdot Structure interaction$

1 Introduction

An abdominal aortic aneurysm (AAA) represents a localized dilation of the central aorta that asymptomatically develops over long periods of time until sudden rupture. Upon rupture, AAA patients have a mortality rate of over 80% (Kühnl et al. 2017). The asymptomatic nature of AAAs complicates diagnosis and detection (Moxon et al. 2010); thus, a proper understanding of the AAA development can lead to diagnostic tools and assessments to aid in the management of this disease. A majority of AAAs (over 75% according to Harter et al. (1982)) contain a layer called an intraluminal thrombus (ILT). The ILTs play a key chemo-mechanical role

in the evolution of AAAs, which is still not fully understood. In particular, in 80% of clinical cases, AAAs were found to rupture in the ILT bearing regions (Silva et al. 2000). Yet, the impact of ILT layer on AAA progression and evolution is highly controversial in the literature, leaving open the question of whether ILT increases or decreases AAA rupture risk (see (Boyd and Intraluminal thrombus, 2021; Wilson et al. 2013) for a comprehensive review on this controversy). Several studies have demonstrated that ILT decreases aortic wall stress, thereby providing a biomechanical advantage by acting as a mechanical buffer (Wang et al. 2002; Haller, et al. 2018). In fact, some numerical studies that compared AAA wall characteristics between aneurysms with and without ILT have found ILT to lower wall stress (Wang et al. 2002; Bluestein et al. 2009; Martino et al. 1998; Georgakarakos et al. 2009; Li et al. 2008a; Mower et al. 1997), suggesting that its presence could prevent AAA rupture. However, ILT has also been shown to create an inflammatory environment by reducing oxygen flux to the aneurysmal wall (Coutard et al. 2010; Lim et al. 2013). The arterial tissue responses to altered oxygenation contribute to decreasing wall strength, due to which AAAs with an ILT were put at



 [⊠] Rana Zakerzadeh zakerzadehr@duq.edu

Department of Engineering, Rangos School of Health Sciences, Duquesne University, 413 Libermann Hall, 600 Forbes Avenue, Pittsburgh, PA 15282, USA

Department of Applied and Computational Mathematics and Statistics, University of Notre Dame, Notre Dame, IN, USA

a greater risk of rupture despite the lower subsequent wall stress (Vorp et al. 1996a; Vorp et al. 1996b). Similarly, it was concluded by Vorp et. al in Vorp et al. (2001); Vorp et al. 1998) that thrombi are detrimental due to the resulting localized hypoxia across the arterial wall. In particular, thick thrombi may exacerbate hypoxic conditions within the wall tissue, which stimulates inflammatory processes and causes neovascularization from the vasa vasorum, altered collagen production, degradation of the extracellular matrix of walls covered by ILT (Lim et al. 2013), and potentially lowering the wall tensile strength (Kazi et al. 2003). The controversy and limited research on the role of ILT in AAA progression and rupture point to a pressing need for more research on the topic. A proper understanding of AAA-ILT behavior could improve the development of diagnostic tools to assess aneurysm cases and potentially reduce the risk of fatalities.

Most computational models of AAAs have focused on the biomechanics of the wall in the absence of blood flow (i.e., (Vorp et al. 1998; Polzer et al. 2012)), although hemodynamics is likely a key factor in the development of AAA (Virag et al. 2015). A patient-specific computational fluid dynamics (CFD) simulation by Zambrano et al. (Zambrano et al. 2016) explored the association between ILT and AAA growth. Their findings suggest that hemodynamic forces and ILT interact with each other and significantly affect AAA expansion, making AAA prognosis a complex problem. The impact of key morphological features of aneurysms on ILT formation is investigated in Bhagavan et al. (2018); however, ILT itself has not been included in this computational model. A few earlier studies that focused on the impact of ILT on the mechanical stress in the AAA wall had some modeling limitations, such as neglecting the interaction with the hemodynamics (Riveros et al. 2015; Polzer et al. 2011; Li et al. 2008b), and sometimes with idealized physical settings, which resulted in relative success (Wang et al. 2002; Sun, et al. 2009; Raptis et al. 2016; Stergiou et al. 2019). Wang et. al (Wang et al. 2002) observed the effects of the ILT on the wall stress in patient-specific AAA geometries using the finite element method (FEM). The conclusion of this work was that the peak wall stress is reduced for all cases with the ILT as compared to the cases without the ILT. A similar study was performed by Haller et. al (Haller, et al. 2018), where it was discussed that the peak wall stress is reduced for ILT-including cases. Nevertheless, it was found that the increased thrombus burden is associated with AAA rupture at smaller diameters. The above-mentioned numerical studies of the AAA wall stress calculation were based on the patient-specific image reconstruction but assumed uniform pressure inside the AAA, and did not account for flow induced stresses within the AAA, or for the different flow patterns in the presence of ILT. Recently, a coupled model for the interaction between an AAA, ILT, and blood flow was used to investigate the role of ILT on the risk of AAA rupture as assessed by the peak wall stress by Bukac et al. (Bukač and Shadden 2021). The AAA and ILT were described using a poroelastic model for ILT, and simulations were performed in patient-specific models. However, the oxygen transport to the wall was not considered.

Therefore, although the relationship between ILT and AAA wall stress has been thoroughly investigated in prior research (Haller, et al. 2018; Zambrano et al. 2016; Bhagavan et al. 2018; Polzer et al. 2011; Li et al. 2008b; Raptis et al. 2016; Bukač and Shadden 2021), many of them did not include the interaction with blood flow in their computational methodology, or used modeling assumptions, such as the idealized geometries or simplified wall material models. Furthermore, as noted by Wang et. al (Wang et al. 2002), the incorporation of oxygen diffusion is still lacking in the models that assess the effects of ILT on wall stress and rupture. In the very few cases that considered the coupling between hemodynamics and mass transport (i.e., (Sun, et al. 2009; Zakerzadeh et al. 2021)), the arterial wall was modeled as a rigid material. Hence, the relationship between ILT and oxygen flow is not well described and there has been limited research of thrombus-mediated effects on mass transport in AAAs. To date, there are no computational models that capture both the oxygen flow inside of an AAA and its deformation coupled with blood flow dynamics.

In our previous studies on this subject, we identified parameters for which AAA oxygen transport is most relevant (Zakerzadeh et al. 2021; Zakerzadeh et al. 2020; Carbino, et al. 2022). In particular, in Zakerzadeh et al. (2021) the effects of vasa vasorum flow, kinematic diffusivities within the AAA tissue, and oxygen consumption in the arterial wall on concentrations within the tissue were analyzed in an idealized AAA model. In (Zakerzadeh et al. 2020), the impact of a porous ILT and therefore the filtration velocities on the oxygen flow was illustrated. In particular, we investigated how ILT properties, such as permeability and diffusivity, affect the risk of oxygen deprivation in patient-specific AAA geometries. We also recently explored the connection between ILT length and thickness with local hypoxia using a comprehensive geometrical study in an idealized AAA (Carbino, et al. 2022). We have shown that ILT geometry variations can have the largest effect on oxygen transport and can cause further hypoxia and weakening of the wall where the ILT is present. However, the predictions of oxygen concentration in all these aforementioned studies are obtained using a rigid wall assumption for the arterial wall, which limited us to investigate the effect of ILT on the wall stress.

Therefore, in this study, we sought to explore the association between ILT, mechanical stresses, and oxygen flow in different geometries of patient-specific AAAs with varying ILT shapes and thicknesses. The objective is to investigate how ILT presence affect the transport of oxygen to the aortic wall, as well as tissue deformation,



and to quantify the ILT contribution on model outcome. To achieve this, we develop a coupled blood flow–tissue deformation–oxygen transport computational framework by combining a fluid–structure interaction (FSI) model with a mass transport model in AAA. This physiologically realistic framework is used to analyze the wall stress and oxygen concentration in patient-specific AAA models, based on which we assess the role of ILT on model predictions.

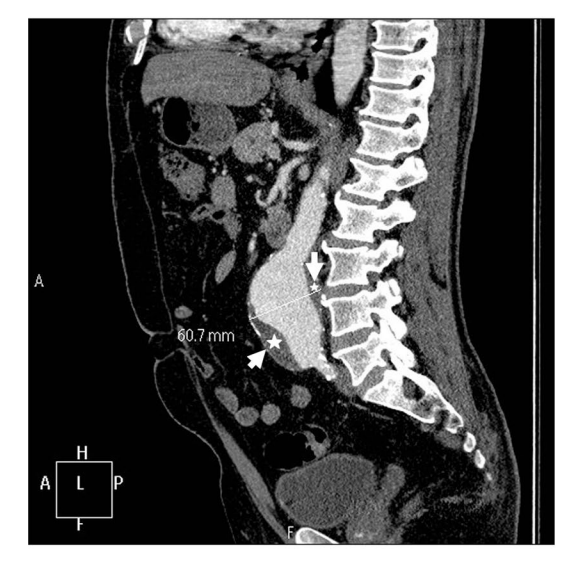
The central goal of this work is to simulate and examine patient-specific cases of AAAs and analyze the extent to which ILT presence influences aneurysmal wall stresses that are associated with rupture, as well as oxygen concentration values to measure hypoxia. To our knowledge, this is the first study to evaluate the effect of ILT on both oxygen flow and wall stress in an actual 3D reconstructed patient-specific AAA model. The close dependence between hemodynamics, oxygen transport in the presence of ILT, and AAA wall stress indicates the importance of studying them together, but previous studies focus on relationships between just two of these three factors. In contrast, this study analyzes all three factors using patient-specific computer simulations of AAA. Three different patient-specific geometries are adopted, and two models are created for each patient: one with the presence of the ILT and one without ILT. Numerical simulations in the presence and absence of ILT are performed and results for stress and deformation patterns, oxygen transport measures, and blood flow velocity fields are presented and compared.

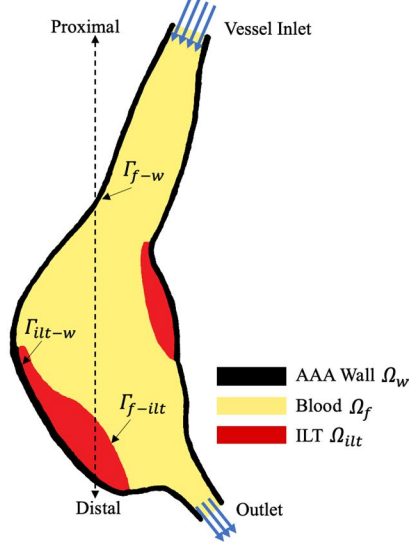
2 Formulation and methods

In this section, we summarize the mathematical model and governing equations to simulate the blood flow, oxygen transport, and wall mechanics of the patient-specific 3D AAA models. A schematic overview of the model under consideration is presented in Fig. 1. Subscripts f, w, and ilt denote the blood flow in the lumen, AAA wall, and ILT medium, respectively. In particular, we examine three patient-specific AAA geometries shown in Fig. 2, where each included a thrombus of a different shape and thickness. The geometries are reconstructed from computed tomographic (CT) scans image data, and the SimVascular software (Updegrove et al. 2017) is used to segment the lumen and ILT domains. The arterial wall is extruded from the inner vessel wall defined in the image data using a constant thickness of 2 mm. The three domains result from this construction, lumen, ILT, and arterial wall, are meshed in the open-source software, Gmsh (Geuzaine and Remacle 2009), using tetrahedral elements.

Two models are created for each patient: one with ILT and one with the same geometry of the arterial wall but without ILT. The reconstructed AAA including ILT is shown for each subject in Fig. 2. The ILT is shown in red, and the AAA and lumen are shown in gray. By visual comparison of geometries, patient 1 contains the largest aneurysm and the longest and thickest ILT, and the shape of it resembles an elongated sac, while patients 2 and 3 have relatively similar ILTs in thickness and length. Patient 2 has a moderately large aneurysm, while patient 3 has the smallest aneurysm diameter, as well as the smallest ILT in length and in thickness. The ILT in the first AAA case occupies a significant part of the aneurysm volume. In patient 2, the aneurysm is

Fig. 1 A sagittal CT image of a human AAA demonstrating the thrombus-covered region with dark gray (star and arrowhead), and the location of maximal aneurysm diameter (left), and a schematic of the patient-specific three-dimensional model of an AAA, Ω and Γ indicates volume and boundary surface, respectively. CT image is taken from (Chiu et al. 2014)







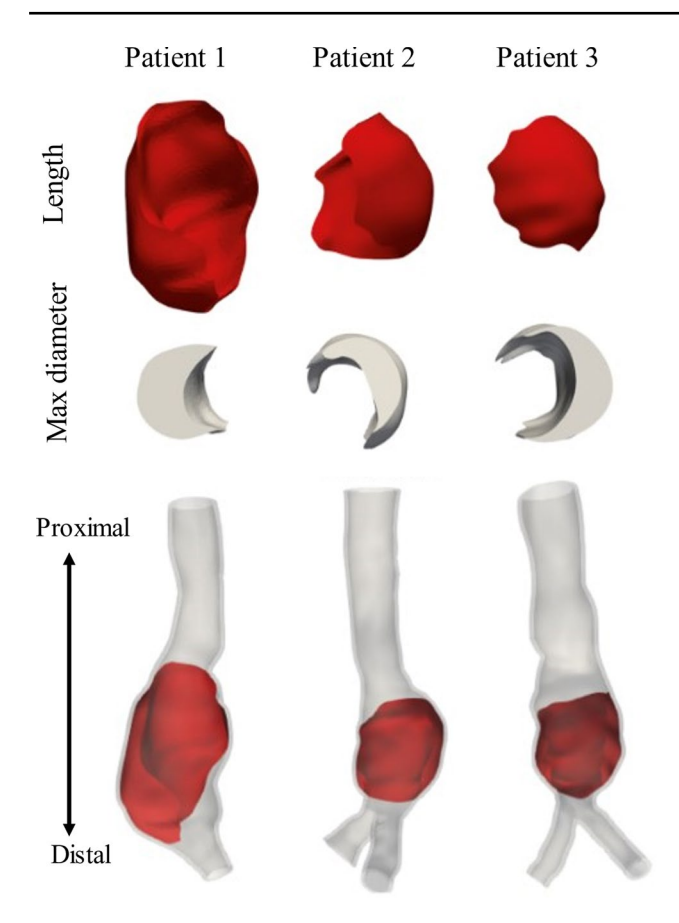


Fig. 2 Three patient-specific AAA geometries used in numerical simulations. The lumen and the arterial wall are shown in gray, while the ILT is shown in red. Two models are created for each patient: one with the presence of the ILT and one that lacks the ILT. Each geometry is quite irregular and is different from patient to patient

spherical in shape and the ILT mostly occupies the upper half of it. The bifurcation was not considered in the geometry of patient 1, while the second two patients have the bifurcation included. The geometric features of AAA and contained ILT varied widely among selected subjects and are given in Table 1. The volume of AAA is defined as the volume contained within the 3D reconstructed inner wall surface, while the volume of ILT is calculated as the volume contained between the 3D reconstructed inner AAA wall and the 3D reconstructed lumen.

We are particularly interested in understanding the threeway interaction between the ILT, arterial walls, and blood flow. In the following, we review the models used in this study for the lumen, as well as the ILT and arterial wall domains.

2.1 Blood flow in the lumen

Blood flow in the lumen is assumed to behave as a Newtonian incompressible viscous fluid and is modeled by the Navier–Stokes equations. Considering blood as a Newtonian fluid is a reasonable approximation in AAA given the rates of shear typically found in the human aorta (Fournier 2017). Blood flow is also considered to be laminar and steady. We found the hemodynamic information as well as the peak wall stress and wall deformation obtained from the steady-state simulations to be very similar to transient flow rate waveforms. More discussion on this comparison is provided in Sect. 4.2.

Therefore, the flow inside the lumen is described by:

$$\rho_f(U_f.\nabla U_f) = \nabla.\sigma_f \text{ in } \Omega_f$$
(1)

$$\nabla . U_f = 0 \text{ in } \Omega_f \tag{2}$$

 U_f and ρ_f stand for the fluid velocity vector field in the lumen and the blood density, respectively. $\sigma_f = -p_f \mathbf{I} + 2\mu_f \mathbf{D}(U_f)$ is the fluid Cauchy stress tensor where p_f is fluid pressure in the lumen, μ_f denotes blood dynamic viscosity, and the symmetric part of the fluid velocity gradient is defined as $\mathbf{D}(U_f) = \frac{1}{2}(\nabla U_f + \nabla U_f^T)$.

The oxygen transfer in the lumen is coupled with the blood flow equations and governed by the convection—diffusion equation as follows:

$$\nabla \cdot \left(-D_f \nabla C_f + U_f C_f \right) = 0 \text{ in } \Omega_f \tag{3}$$

 C_f stands for the oxygen concentration in the lumen and D_f denotes the kinematic diffusivity of the oxygen transport in the blood. Here, the effect of oxygen binding to hemoglobin on oxygen concentrations in the lumen is neglected, as the focus here is on comparisons of relative transport over the

Table 1 Characteristics of the patients including geometric features of three AAAs and contained ILT

Cases	ILT Thickness (maximum) × 10 ⁻² (m)	ILT Length × 10 ⁻² (m)	ILT Vol- ume × 10 ⁻⁶ (m ³)	AAA Length × 10 ⁻² (m)	AAA Volume $\times 10^{-6}$ (m ³)	AAA Diameter (maximum) × 10 ⁻² (m)
Patient 1	1.74	8.16	45.7	8.23	102.5	4.80
Patient 2	1.35	5.25	25.0	7.00	82.5	5.00
Patient 3	1.27	4.95	17.0	6.50	61.1	4.22



AAA wall. A summary of all fluid flow model parameters is provided in Table 2.

2.2 Aortic wall and intraluminal thrombus

Both ILT and AAA wall are assumed to be hyperelastic, homogenous, incompressible, and isotropic materials. The governing equation for both domains is the momentum conservation given by:

$$\nabla . (\boldsymbol{\sigma}^{w}) = 0 \text{ in } \Omega_{w} \tag{4}$$

$$\nabla \cdot (\boldsymbol{\sigma}^{ilt}) = 0 \text{ in } \Omega_{ilt} \tag{5}$$

where σ^w and σ^{ilt} represent the solid structure stress tensors for wall and ILT, respectively. We adopt the constitutive models for the AAA wall and ILT to be second order Mooney–Rivlin material models, for which the functional form of strain energy function (W) is defined by:

$$W_{w} = \alpha (I_{\boldsymbol{B}} - 3) + \beta (I_{\boldsymbol{B}} - 3)^{2} \tag{6}$$

$$W_{ilt} = c_1 (II_B - 3) + c_2 (II_B - 3)^2, \tag{7}$$

where α , β , c_1 , and c_2 are constant material parameters for the wall and ILT, and I_B and II_B are the first and second invariants of the left Cauchy–Green deformation tensor B, respectively. The values for these constants and corresponding references are obtained using population averages and provided in Table 2. The oxygen transport in the wall is described by the diffusion–reaction equation, given by:

$$\nabla \cdot \left(-D_w \nabla C_w \right) = r C_w \text{ in } \Omega_w \tag{8}$$

where C_w is defined as the oxygen concentration in the arterial wall and D_w is the oxygen diffusivity through the arterial wall tissue. The term rC_w is the reaction term, accounting for the metabolic consumption of oxygen in cell metabolism, where r is defined as the oxygen reaction rate constant

(Iannetti et al. 2016). The ILT is assumed to be permeable to the transport of oxygen molecules through diffusion via the canaliculi network without any smooth muscle cells to consume oxygen. Therefore, no reaction term is considered in the thrombus. The oxygen transport in the ILT is modeled by the diffusion equation:

$$\Delta \cdot \left(-D_{ilt} \nabla C_{ilt} \right) = 0 \text{ in } \Omega_{ilt} \tag{9}$$

Here D_{ilt} and C_{ilt} stand for the oxygen diffusivity through the ILT and oxygen concentration in the ILT, respectively. It should be noted that the arterial wall and ILT are modeled as tissues impermeable to interstitial fluid flow but permeable to oxygen transport. Therefore, for oxygen transfer in the ILT and arterial wall, the effect of convective transport is ignored. Although ILT has a porous structure arising from its highly porous canalicular network (Adolph et al. 1997), neglecting the contribution of convective oxygen transport due to interstitial fluid flow (i.e., the movement of the fluid through the extracellular matrix of the tissue) has been justified in Polzer et al. (2011); Polzer and Bursa 2010) where the stress fields in the aneurysmal wall changed negligibly when a poroelastic model for ILT was used. Similar conclusions were obtained in Ayyalasomayajula et al. (2010) where simulations were performed in order to compare poroelastic and impermeable ILT models, and the ILT permeability was found to have minimal effect on interstitial velocities that have been associated with driving oxygen transport in the ILT and arterial wall. We previously explored the effect of porous ILT on oxygen transport and our findings suggest that the effect of porosity of ILT on oxygen transport within AAA is small for the reported physiological range of ILT permeability (Zakerzadeh et al. 2020).

2.3 Boundary conditions and physical parameters

In this section, we summarize the prescribed conditions over the coupled system boundaries. The following inflow and outflow boundary conditions are applied to the fluid

Table 2 Material properties and values of physical parameters in simulation

Domain	Parameter Description	Parameter Value 1050 kg/m ³			
Blood	Density ρ_f				
	Dynamic viscosity μ_f	0.0035 kg/m.s			
	Oxygen diffusivity D_f	1.6×10^{-9} m ² /s (Rappitsch and Perktold 1996)			
Arterial Wall	Oxygen diffusivity D_w	1.08×10^{-9} m ² /s (Moore and Ethier 1997)			
	Reaction rate r	$8.4 \times 10^{-3} \text{ s}^{-1}$ (Caputo et al. 2013)			
	Mooney–Rivlin hyperelastic constant α	1.74×10^{-3} N/m ² (Raghavan and Vorp 2000)			
	Mooney–Rivlin hyperelastic constant β	1.88×10^{-2} N/m ² (Raghavan and Vorp 2000)			
ILT	Oxygen diffusivity D_{ilt}	1.34×10^{-9} m ² /s (Sun, et al. 2009)			
	Mooney–Rivlin hyperelastic constant c ₁	$7.98 \times 10^{-4} \text{ N/m}^2 \text{ (Geest et al. 2006)}$			
	Mooney–Rivlin hyperelastic constant c_2	$8.71 \times 10^{-4} \text{ N/m}^2 \text{ (Geest et al. 2006)}$			



cross-sectional areas at the proximal and distal regions, respectively (the anatomical orientations depicted in Fig. 1). A uniform systolic pressure of $p_f^{in} = 130$ mmHg is applied as a boundary condition at the inlet of the fluid domain. This value is in the range of recorded data for the average in vivo luminal pressure values reproduced from Vosse, F.N.v.d. and N. Stergiopulos (2011). At the outlet of the fluid domain, a mass flow rate of 0.075 kg/s is applied which is obtained using the peak systole value of the flow rate waveform for a cardiac cycle presented in Reymond et al. (2009), and is in agreement with the experimental measurements that have shown that the maximum blood flow rate of the abdominal aorta is about 4.5 ± 0.9 L/min, as reported in Amanuma et al. (1992) and (Cheng et al. 2015). Using these information for static systolic pressure at the inlet and flow rate at the outlets, the obtained luminal velocity value matches the typical peak systolic blood velocity of 0.23 m/s within the aneurysm (Swillens, A.l et al. 2008). Moreover, the resulting Reynolds number of 1600, representing typical physiologic peak flow conditions during the cardiac cycle, is within the realistic range for Reynolds numbers in the abdominal aorta at rest (Ku 1997).

The fixed support condition is assigned at inlet and outlet for AAA wall ending cross sections. In this way, all the degrees of freedom are set to zero and the arterial wall cross sections are prevented from moving and deforming. Moreover, the outer AAA wall is prescribed to be traction-free with zero external pressure imposed on the surface.

The inlet oxygen partial pressure is considered a uniform 100 mmHg corresponding to the oxygen saturation of 97.7%. Therefore, the oxygen concentration of C_f^{in} =5.12×10⁻³ kg/ m^3 at the lumen inlet Γ_f^{in} is obtained by using the inlet partial pressure and molar mass of oxygen. At the model outlet Γ_f^{out} , the reference pressure value is prescribed, which can be arbitrarily set for incompressible flow. On the exterior of the arterial wall, the influence of the vasa vasorum is modeled by imposing the partial pressure of oxygen. Experimental studies showed that the level of adventitial oxygen tension is about one half of the oxygen tension in blood (Buerk and Goldstick 1982, 1986); therefore, the abluminal wall partial pressure is fixed at 50 mmHg to model the oxygen transported by the vasa vasorum (Kemmerling and Peattie 2018). At the cross-sectional areas of the wall representing the ends of the vascular domain, a zero-flux condition on the surface normal direction is prescribed.

At the cross-sectional areas of the wall representing the ends of the vascular domain, a zero-flux condition on the surface normal direction denoted by n is prescribed. Conservative interface flux conditions for the oxygen flow are employed at the ILT-wall (Γ_{ilt-w}), lumen and wall Γ_{f-w} , and ILT-lumen (Γ_{f-ilt}) interfaces, and a continuity condition is assumed between the boundaries. Therefore, the model is

complemented by the following concentration and flux interface conditions.

$$C_f = C_w, (U_f C_f - D_f \nabla C_f).\mathbf{n} = (-D_w \cdot \nabla C_w).\mathbf{n}$$
 on Γ_{f-w}

$$C_f = C_{ilt}, (U_f C_f - D_f \nabla C_f).\mathbf{n} = (-D_{ilt} \cdot \nabla C_{ilt}).\mathbf{n} \text{ on } \Gamma_{f-ilt}$$

$$C_{ilt} = C_w, \ \left(-D_{ilt} \cdot \nabla C_{ilt}\right).\mathbf{n} = \left(-D_w \cdot \nabla C_w\right).\mathbf{n} \text{ on } \Gamma_{ilt-w}$$

$$(10)$$

Fluid–structure interfaces were defined on the combined wall-lumen (Γ_{f-w}) and ILT-lumen (Γ_{f-ilt}) interfaces. As for the FSI boundary conditions, it is assumed that the displacement of the interface is the same for the fluid and solid domains. Moreover, the no-slip wall condition is defined at the FSI surfaces. Finally, normal stress equilibrium conditions are assumed at all interfaces, and a bonded contact constraint condition is assumed at the ILT-wall interface (Γ_{ilt-w}).

2.4 Computational modeling details

The computational framework has three components to simulate hemodynamics, aortic wall deformation, and oxygen transport. The coupled model is implemented in ANSYS® Workbench software (v. 21, ANSYS Inc., Canonsburg, PA, USA). More precisely, the blood flow dynamics and oxygen mass transport are defined in ANSYS CFX, while the wall mechanics is modeled and solved in ANSYS Mechanical. The fluid and structural components are joined along a single fluid–solid interface which is defined on the luminal surface and inside of the arterial wall and ILT, namely $\Gamma_{f-ilt} \cup \Gamma_{f-w}$ boundary. Fluid flow and structural mechanics interact via this coupling region, whose behavior is dictated by the ANSYS Workbench platform System Coupling module (Chimakurthi et al. 2018).

The equations and conditions listed in Sects. 2.1–2.3 are implemented in a fully coupled system. The steady-state, two-way FSI-oxygen transport simulations are performed. Continuity and Navier-Stokes equations governing the blood flow, as well as diffusion-reaction equations for oxygen transport are solved in CFX, and ILT and aortic wall deformation equations are solved in mechanical solver. For the blood flow and oxygen transport, the finite volume method and a fully coupled solver for the pressure and velocity are used, whereas for the solid domain a three-dimensional finite element method is employed. The System Coupling component controls the execution and convergence of fluid and solid simulations and solves fluid flow field and solid structure domains separately and in a sequential fashion, starting from the blood flow and oxygen transport simulations. In particular, the module first solves the fluid component in ANSYS CFX to obtain the oxygen concentration distribution



as well as the non-uniform pressure distribution and flow velocity in the lumen.

The Laplace operator in the fluid momentum and oxygen transport equations is approximated by a centered scheme, and a second-order upwind interpolation scheme is applied for spatial discretization of convective terms in momentum equations within fluid zone. The convective term in the Navier-Stokes equations is linearized by the Picard iterations ("ANSYS CFX-Solver Theory Guide", ANSYS Inc., 2010). The pressure variable in the Navier-Stokes equations is evaluated at the same nodes of the velocity field. The DNS method for laminar flow is employed for the solution, as the flow in the AAA demonstrated no turbulent characteristics ($Re_{max} = 1600$). The blood flow and oxygen transport equations are solved simultaneously in a monolithic linear system. The system is then solved using an algebraic multigrid method exploiting incomplete LU factorization as smoother. The convergence criteria of the ANSYS CFX are set to 10⁻⁵ for the normalized residuals of the global linear system of equations for the mass and momentum. The obtained non-uniform pressure loads from the blood flow are then transferred and applied to the solid component, i.e., arterial wall and ILT, through the fluid-solid interface and the wall displacement and corresponding stresses are solved in ANSYS Mechanical. The displacement of the solid walls was transferred to the CFX, and fluid problem is solved for convergence. These stagger loops are reinitialized with the new deformed mesh that occurs from the solid deformation. The coupling iterations are repeated until the convergence is reached, i.e., the interactions between fluid and structural components are converged. In System Coupling, a maximum root-mean-square (RMS) residual of 0.01 must be reached for both fluid and solid domains to ensure the convergence of the solution of the coupled algorithm.

Using this computational framework, the association between mechanical stresses and oxygen starvation in the wall in different geometries of aneurysms with varying ILT shapes and thicknesses is explored. Computational analysis is performed on three patient-specific AAA geometries (Fig. 2) to simulate hemodynamics, aortic wall dynamics, and oxygen transport. Two analyses are carried out for each patient in order to estimate the effect of ILT inclusion on stress distribution and oxygen flow within the aneurysmal wall: one simulation is performed with the 3D reconstructed ILT included in the geometry, while in the other simulation the ILT was excluded. For each patient-specific AAA model, a mesh convergence study is carried out to assure an optimally sized mesh. This is accomplished by increasing the number of elements until the maximum wall principal stress and the wall displacement distribution does not change appreciably (relative error less than 5%). More precisely, stress and displacement analyses with coarser and finer meshes showed negligible error when comparing the

von Mises stress, maximum principal stress, and total displacement patterns. The fluid flow solution is also considered mesh independent for an error lower than 5% in terms of velocity and pressure. The elemental composition of the patient-specific geometries for resulting meshes that guaranteed mesh density independence is summarized in Table 3. The geometries are split into linear tetrahedral elements in order to perform the simulations.

3 Results and discussion

In this section, we present the results of the numerical simulations in three different patient-specific models with an ILT. Variables for blood flow fields, wall deformation patterns and stress mappings are extracted for each simulation. Outcomes are also presented for the amount and distribution of the oxygen within the AAA. These results are compared to the ones obtained with the same AAA geometry but lacking the ILT.

3.1 Hemodynamic patterns in AAA

The simulation results provide qualitative and quantitative prediction of blood flow patterns and pressure distribution in the AAA models. The velocity streamlines depicted in Fig. 3 show some similarities and differences in the blood flow pattern between AAAs that contain an ILT deposition from those that did not include it. In all AAAs, regardless of the presence of the ILT, the streamlines indicate a helical pattern at the AAA bulge region. The spatial variation of blood velocity in the aneurysm shows that ILT removal impacts hemodynamics in the lumen and significant differences are noted when comparing cases with or without the ILT for each patient. Our findings revealed that the presence of an ILT resulted in the weakening of flow recirculation in the aneurysm sac and shifted the flow fields toward the center of the aorta. A larger recirculation vortex is observed when ILT is excluded in each case (Fig. 3). The velocity accelerates at the outlets where the diameter of the lumen is smaller. Flow recirculation and complex flow trajectories within the AAA are commonly observed among all cases with and without ILT; however, the recirculation zones are larger when ILT is removed, as the diameter of the lumen enlarges at this portion. In particular, it is clear that the

Table 3 Mesh characteristics for different cases

Cases	Number of elements	Blood	ILT	Arterial wall
Patient 1		120,873	110,074	80,250
Patient 2		273,799	69,859	128,684
Patient 3		393,042	92,555	189,781



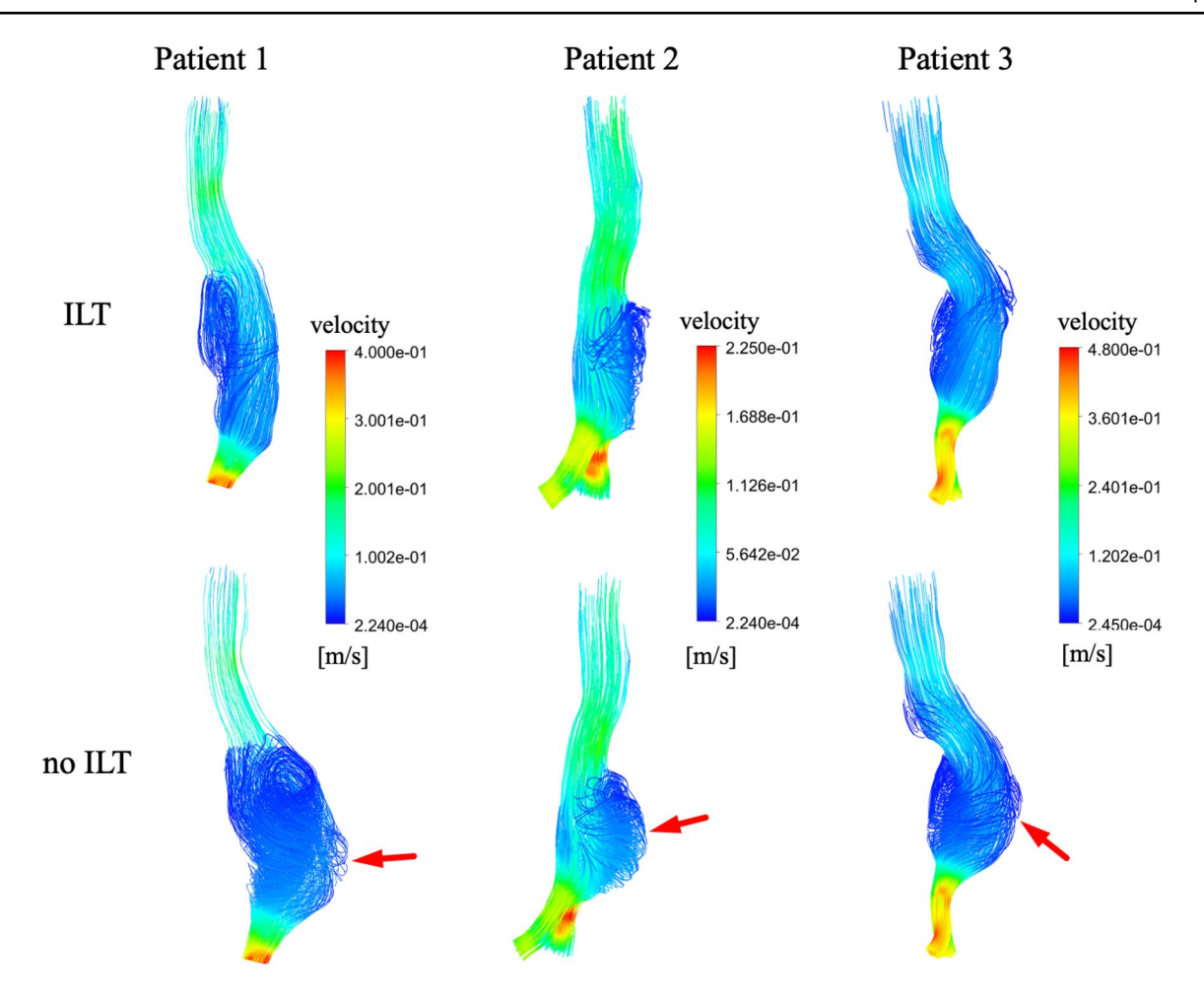


Fig. 3 Comparison of 3D flow pattern using velocity streamlines in the investigated AAA models with and without ILT. Helical flow and strong recirculation are present inside the aneurysm sac. The color bar number represents the velocity magnitude at peak systole; lower

velocity values are represented by colors toward the blue end of the spectrum, whereas red indicates higher values. The red arrows indicate the location of larger recirculation zones in AAA models after ILT removal

presence of a large ILT significantly changes the flow patterns within the AAA lumen by reducing the flow channel. Aneurysm sac diameter, aneurysm shape, and parent artery diameter are other parametric factors that influence the blood flow pattern within an aneurysm. For example, the neck size decides the amount of flow entering in the aneurysm sac and the volume of the aneurysm deciding on how sluggish the flow in the aneurysm sac is. Significant differences in flow pattern (as indicated by the streamlines in Fig. 3) are noted when comparing the case with and without the ILT for each patient.

Moreover, simulation results demonstrate physiologically realistic pressure distribution in the lumen of the three AAAs, with the maximum pressure value around 1.74×10^4 Pa, equivalent to 130 mmHg at the proximal surface. The distribution of the pressure along the lumen for the cases without the ILT is consistent with the cases that include the ILT. It is also found that the pressure distribution in the AAA is highly uniform and the pressure drop between

the two endings of the AAA is minimal (~ 150 –200 Pa) for all cases (pressure contours are not shown here). For the first case with the ILT, the pressure is high along a large portion of the lumen and decreases slightly at the outlet. This behavior is consistent with the case without the ILT. The second case, with and without the ILT, shows a gradual decrease in pressure along the lumen. The third case is similar to the first where the pressure is high along the lumen and decreases at the outlets.

3.2 Effect of the ILT and AAA wall deformation and stresses

From the structural analysis of tissue deformation, three response variables are extracted for each simulation. Namely, we analyzed measures for the arterial wall displacement, as well as the maximum principal stresses (S_{max}) and von Mises stresses (σ_v) distributions on the aortic wall. Moreover, for each individual simulation, the peak maximum principal



stress and the peak von Mises stress within the AAA are recorded and compared in the studied cases, with and without ILT.

The wall total displacement distributions for all three AAA models with an ILT and without an ILT are shown in the top and bottom panels of Fig. 4, respectively. The displacements are visualized on the abluminal surface of the arterial wall. In all patients, the presence of the ILT reduced the displacements of the arterial wall within the aneurysmal region, while the corresponding displacements increase significantly when the ILT is removed. From Fig. 4, the maximum displacement is computed and compared. It has been observed that the maximum displacement increases with the removal of the ILT. Specifically, the maximum displacement in patient 1 with the ILT is 1.46 mm and 2.05 mm without the ILT. A stark difference between the maximum displacements is shown in patient 2 where the maximum wall displacement is 1.39 mm with the ILT and 3.41 mm without the ILT. A similar pattern is shown in patient 3 with a maximum displacement of 1.26 mm with the ILT, while the lack of ILT shows a max displacement of 2.58 mm. Furthermore, our results revealed that total displacement of the aneurysmal wall is strongly dependent on location, as well as the presence of the ILT. Namely, as shown in Fig. 4, the displacements are more pronounced within the AAA bulge, and the greatest point of wall deformation is found on the bulge for all the cases. However, for cases with ILT, displacements are larger near the areas within the bulge opposite to the ILT region, where diameter variations are noticeable. Moreover, the maximum displacement varied greatly among the cases, i.e., patient 2 with a small ILT displays the peak wall displacement significantly higher than that of patient 1 with a large ILT. However, no significant differences appear for the total wall displacement when the results between the cases without ILT are compared.

To further investigate the effects of the ILT on AAA mechanics, in addition to the contour plots showing the wall displacement distribution (Fig. 4), we extracted from each patient the distribution of von Mises stresses and their maximum value, as well as the maximum principal stress on the aneurysmal wall. Areas of peak stress on or immediately adjacent to the fixed ends were ignored and the next highest

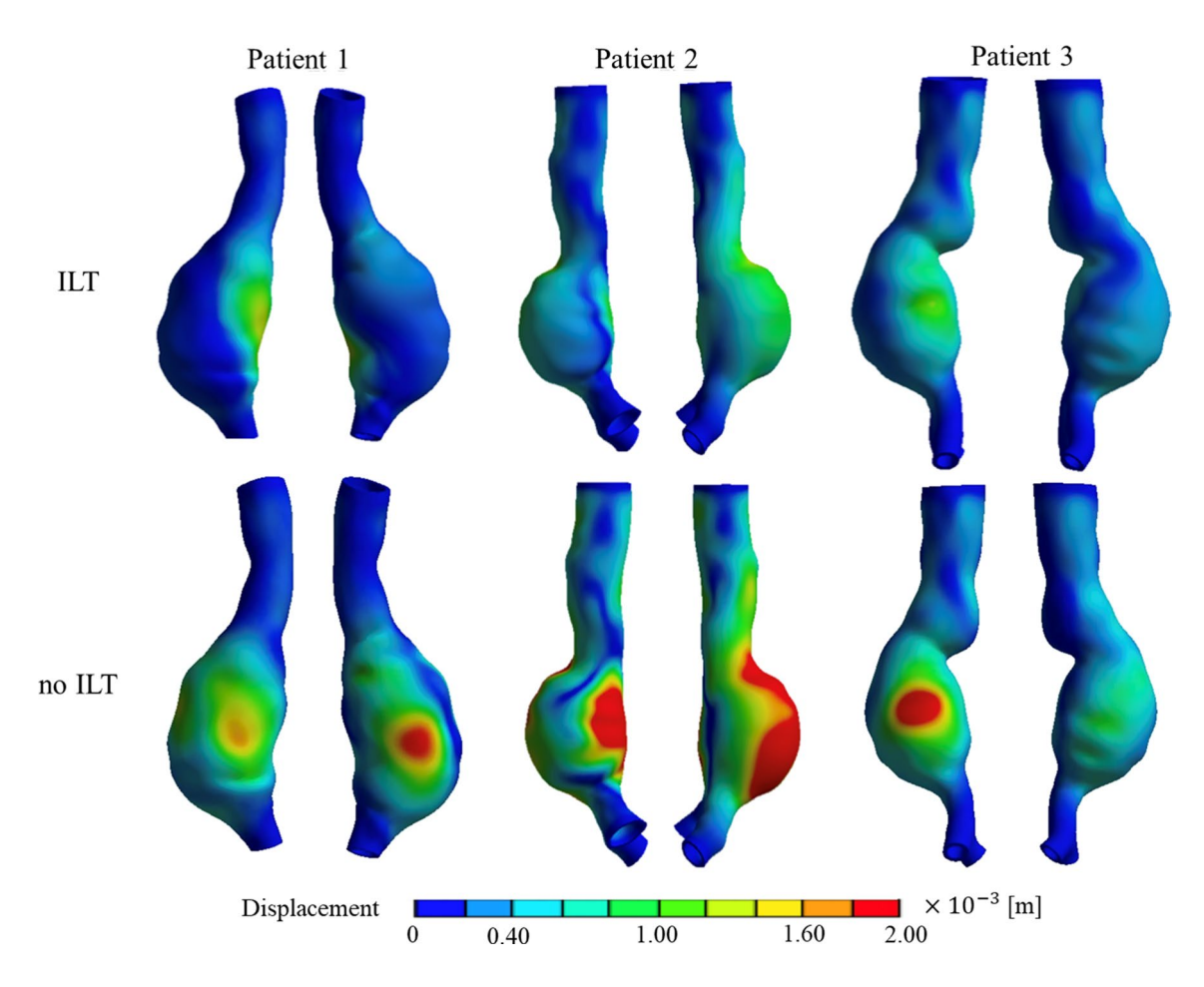


Fig. 4 Views of the total displacement on the exterior of the AAA wall in both the presence and absence of the ILT among the patients. In all cases, the presence of the ILT (top row) reduced the overall displacement pattern of the arterial wall and its maximum value



area used to mitigate boundary effects. The symbol S_{max} indicates the maximum principal stress also known as the peak wall stress defined as $S_{max} = max\{S_1, S_2, S_3\}$, where S_1, S_2 , and S_3 are principal stresses and σ_v denotes von Mises stress. The von Mises stress is a measure of maximum principal stresses and is calculated by using the equation $\sigma_v = \sqrt{\frac{1}{2} \left\{ (S_1 - S_2)^2 + \left(S_3 - S_2 \right)^2 + (S_1 - S_3)^2 \right\}}$. The distribution of the maximum principal stress along the arterial wall in the presence and absence of the ILT is visualized in Fig. 5. Wall von Mises stress distributions in all three AAA models of varying geometry studied are depicted in Fig. 6. The upper row of aforementioned figures depicts the AAAs with the ILT, while the bottom row depicts the AAAs without the thrombus.

Results in Fig. 5 illustrate that similar to the maximum displacement pattern described previously in Fig. 4, the maximum principal stress increases with the removal of the ILT. The AAAs without the ILT show higher levels of stresses indicated by the red colors at the area of the bulge. The cases with the ILT indicate reduced levels of stress as compared to the same AAA without the ILT. Also,

significant differences are found in the maximal principal stress levels between the AAA cases. More precisely, patient 1 shows a maximum principal stress of 0.444 MPa with the presence of the ILT, whereas the peak of maximum principal stress is 0.473 MPa without the ILT. A larger contrast between the S_{max} values is shown in patient 2 where the peak maximum principal stress with and without the ILT is 0.443 MPa and 0.820 MPa, respectively. The peak value of maximum principal stress in patient 3 in the presence of the ILT is 0.382 MPa and 0.560 MPa with the lack of the ILT. The peak maximum principal stresses S_{max} for each of the simulations are listed in Table 4.

Moreover, the von Mises stress distributions are shown in Fig. 6 for each AAA with and without ILT included in the analysis. As expected, there is a strong correlation between aortic wall displacement and distribution of von Mises stresses. It is revealed that peak σ_{ν} appears at the area of maximum deformation of the arterial wall. Based on the three aneurysms studied, it appears that the presence of ILT significantly changes the stress distribution patterns and also reduces the von Mises stresses (Fig. 6, AAA without ILT versus AAA with ILT). The numerical simulations of an AAA with ILT

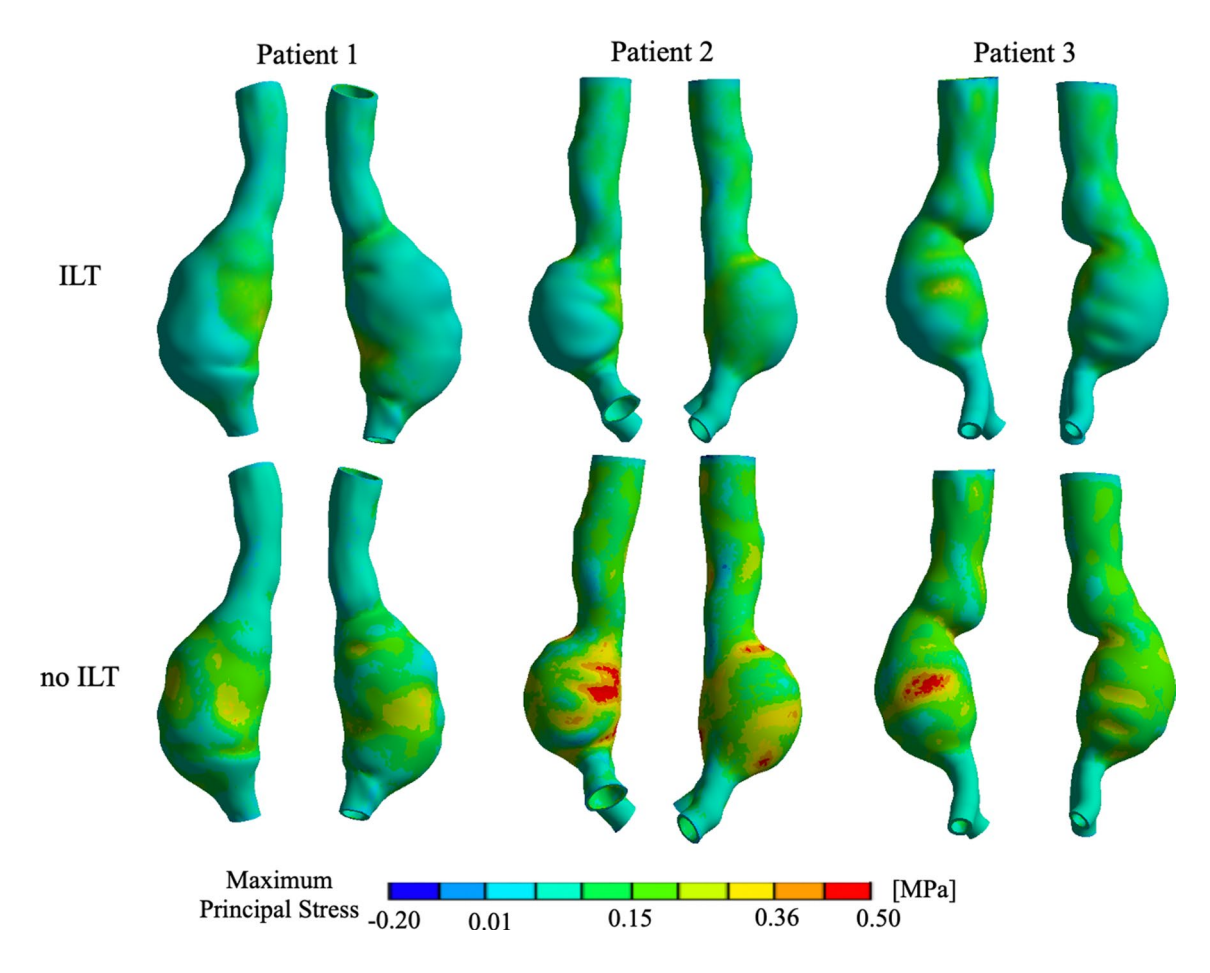


Fig. 5 Views of maximum principal stress distributions throughout the AAA wall surface for AAA models with ILT (top row) and without ILT (bottom row) for three patients. Cases with the ILT indicate reduced levels of stress as compared to the same case without the ILT



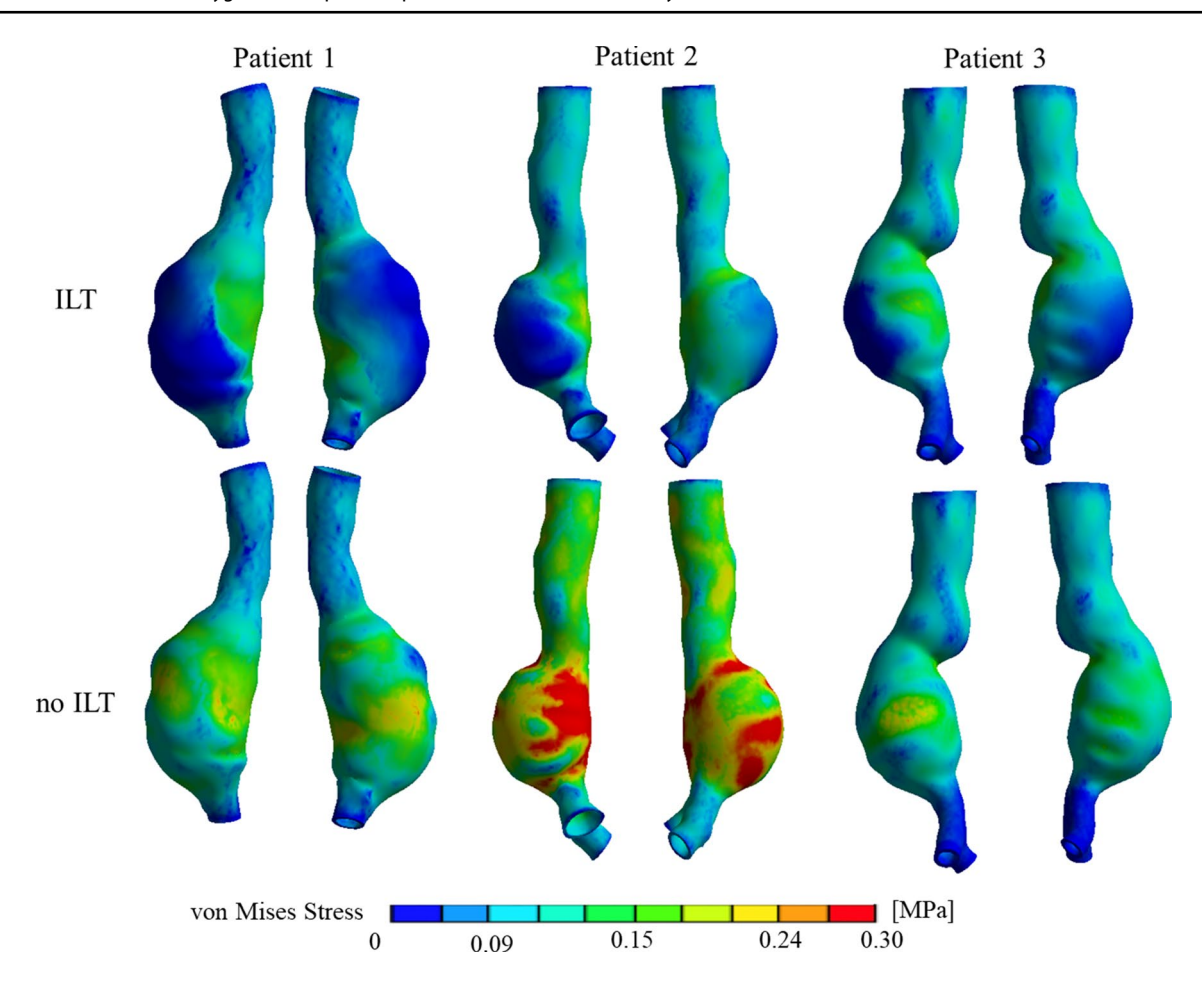


Fig. 6 Comparison of the wall von Mises stress distribution contours between AAA models with an ILT (top row) and without an ILT (bottom row) of three patients. Cases with the ILT indicate reduced levels of stress as compared to the same case without the ILT

Table 4 Comparison of simulation results for von Mises stress, maximum principal stress, and volumetric average of oxygen concentration in the arterial wall in each patient with and without ILT

Cases	Without ILT			With-ILT			Percent Change		
	$\sigma_{\nu}(\text{MPa})$	S _{max} (MPa)	$ \overline{C_w}(\text{kg/m}^3) \times 10^{-3} $	$\sigma_{v}(MPa)$	$S_{max}(MPa)$	$ \overline{C_w}(\text{kg/m}^3) \times 10^{-3} $	$\overline{\delta_{\sigma_{_{\!\scriptscriptstyle u}}}(\%)}$	$\delta_{S_{max}}(\%)$	$\delta_{\overline{C_w}}(\%)$
Patient 1	0.322	0.473	3.68	0.222	0.444	3.29	31.1	6.13	10.63
Patient 2	0.481	0.820	3.73	0.261	0.443	3.53	45.7	46.0	5.39
Patient 3	0.283	0.560	3.72	0.215	0.382	3.54	24.0	31.8	5.06

included clearly indicate reduced stresses at the location of the ILT as compared to the simulation of the same aneurysm without the ILT. Therefore, it is again revealed that the σ_{ν} values are affected by the presence or absence of the ILT. However, the peak σ_{ν} values for both cases occur at the region of the bulge. It should be noted that the 'region of the bulge' refers to the whole section of the artery where the aneurysm is. We also observe that when ILT is included, the area opposite to the ILT in the vessel will begin experiencing more pressure and stress, and therefore peak stress occurs again in the bulge region opposite to the ILT. The location where the peak σ_{ν} stress occurs changes dramatically with the ILT "shielding"

what would otherwise be the location of peak wall stress. In the presence of ILT, the peak σ_{ν} occurs in the posterior region. In the absence of ILT the same region exhibits elevated stress; however, the σ_{ν} occurs in the region otherwise covered by ILT. Compared with the companion models that neglected ILT, the peak von Mises stress in the models including ILT is decreased to varying degrees. For patient 1, the maximum von Mises stress is decreased from 0.333 MPa to 0.222 MPa with the presence of the ILT. Similarly, for the second AAA, the peak of von Mises stress reduced from 0.481 MPa without the ILT to 0.261 MPa with the ILT. The same pattern is exhibited in



patient 3, for the maximum von Mises stress of 0.215 MPa with the ILT and 0.283 MPa without.

Figure 5 and Fig. 6 demonstrate that there is a relation between wall stresses S_{max} and σ_v , and ILT presence in AAA. The ILT plays a large role in the distribution of wall stresses in AAA, and in all cases the presence of ILT markedly altered wall stress distribution. More precisely, in cases with the ILT included, the reduction of wall stress occurs, and the wall stress is also more evenly distributed. Specific values for the maximum principal stresses and von Mises stresses are indicated in Table 4 for each of the patient-specific cases and percentage of differences are calculated. The percentage of change δ between with-ILT measured values and without-ILT values for von 1 principal stress is computed using the formula given by:

$$\delta_{\sigma_{v}} = \left| \frac{\sigma_{v \, w/o \, ILT} - \sigma_{v \, w/ILT}}{\sigma_{v \, w/o \, ILT}} \right| \times 100\%$$

$$\delta_{S_{max}} = \left| \frac{S_{max \, w/oILT} - S_{max \, w/ILT}}{S_{max \, w/oILT}} \right| \times 100\% \tag{11}$$

The calculated percentage of differences indicate that the maximum aneurysm wall principal stress at patient 1 is about 6% higher than when ILT is removed. However, the difference was 46% in patient 2 and about 32% in patient 3. As previously illustrated by the generated plots, the von Mises stresses and their peak value are also reduced with the addition of the ILT. It is observed that for the areas that experience the highest stresses, σ_v nearly doubles when ILT is not present, more precisely, it increases almost 31% for patient 1, 46% for patient 2, and 24% for patient 3 (Table 4). The third column of Table 4 illustrates the comparison for oxygen concentration results and will be explained next, in Sect. 3.3.

3.3 Effect of the ILT and oxygen flow

In this section, the effect of the ILT on AAAs is observed through the variation of the oxygen transport within the AAA domain and in particular the arterial wall. The contours of oxygen concentration distributions are demonstrated in Fig. 7 for each AAA with and without ILT included in the analysis. For each patient, Fig. 7 shows the oxygen distribution in three cross sections along the AAA: one at the

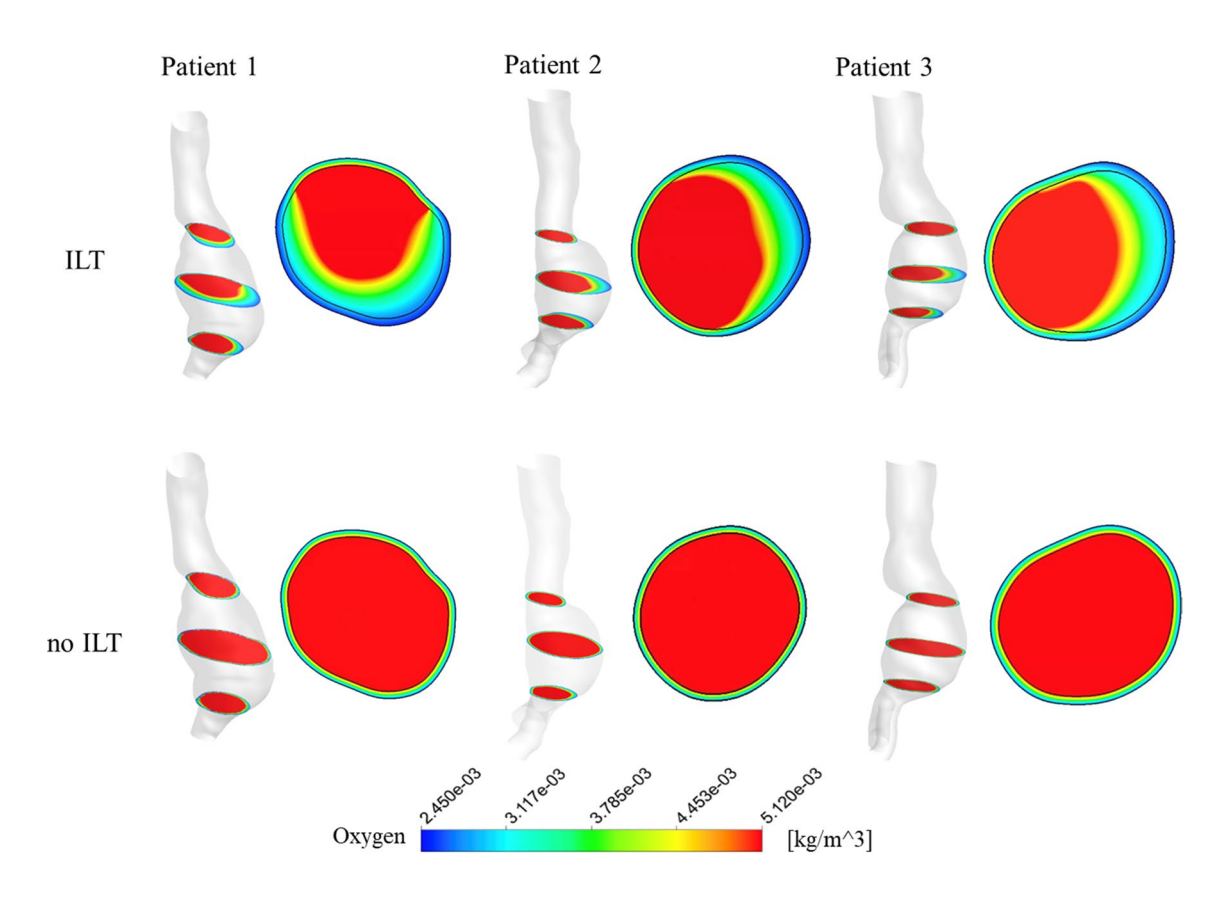


Fig. 7 Oxygen concentration contours at three different cross sections for the three AAA patients, with the concentration contour at the center of AAA bulge magnified. Cross-sectional contours show

significant decrease in concentration in cases with ILT (top row) in comparison with the cases in the same patient without the ILT (bottom row)



proximal neck located at the entrance of the bulge, another one at the center of the AAA bulge, and finally the third cross section is defined at the distal neck at the base of the bulge. The locations of the cross sections are kept consistent for the cases with and without the ILT and oxygen concentrations within the AAA regions are compared.

The highest oxygen concentration is found in the lumen in all cases. This is demonstrated by the dark red color in the center of the AAA (Fig. 7). The oxygen concentration decreases inside the tissue gradually and reaches its minimum value on the wall abluminal surface, which is indicated by the blue color at the edge of the cross section. In fact, the oxygen diffuses across the ILT and arterial wall in the cases that include ILT, while it diffuses only across the arterial wall when ILT is excluded. We observe that the greatest concentration of oxygen on the wall is at the portion where the blood meets the wall. However, for the cases with ILT, the oxygen concentration decreases significantly at the portion of the wall that is in contact with the ILT. In particular, for the patients with an ILT in Fig. 7, a decrease in oxygen concentration along the part of the inner wall which is in contact with ILT is observed, shown by blue color that represents the minimum oxygen concentration. However, the cases without the ILT yield a significantly higher oxygen concentration along the entire interior of the arterial wall, which is close to the concentration of oxygen inside the lumen and is shown by orange-yellow color. This suggests that the concentrations of oxygen are higher along that section. Therefore, the oxygen concentration of the arterial wall decreases in the regions ILT is present. We also observe that the oxygen concentration across the arterial wall decreases in both cases, either without or with the presence of the ILT.

As an indicator of oxygen transported to the AAA wall, we define a measure for the volumetric average of oxygen concentration over the aortic wall domain $\overline{C_w}$ and its percentage of change $\delta_{\overline{C_w}}$ between with-ILT measured values and without-ILT values calculated by Eq. (12) and the corresponding results are reported in Table 4.

$$\overline{C_w} = \frac{\int_{\Omega_w} C_w d\Omega_w}{\int_{\Omega_w} d\Omega_w}$$

$$\delta_{\overline{C_w}} = \left| \frac{\overline{C_{w_w/oILT}} - \overline{C_{w_w/ILT}}}{\overline{C_{w_w/oILT}}} \right| \times 100\%$$
 (12)

Results illustrate that the total oxygen transported to the AAA wall decreases with the presence of the ILT. The patient with a small ILT had also lower oxygen supply within the wall compared with the patient with a large ILT. The average oxygen concentration in the arterial wall for patient 1 is 3.68×10^{-3} kg/m³ without the ILT and 3.29×10^{-3} kg/m³ with the ILT. The percent decrease with the addition of

the ILT is 10.63% for this patient. For patient 2, the percent decrease is calculated to be 5.39%, for the average oxygen concentration of 3.73×10^{-3} kg/m³ without the ILT and 3.53×10^{-3} kg/m³ with the ILT. A similar pattern is observed for patient 3. The oxygen concentration without and with the ILT are 3.72×10^{-3} kg/m³ and 3.54×10^{-3} kg/m³, respectively. The percent decrease for this patient is found to be 5.06%. Therefore, an ILT can decrease oxygen diffusion from the bloodstream to the underlying ILT and aneurysmal wall which is in agreement with observations in Wang et al. (2002).

For each patient, we also plot the concentration of oxygen along the anterior side of the AAA wall, i.e., along the wall behind the ILT. The same region is used in cases when ILT is not present. Figure 8 shows the comparison of the concentration obtained in models with and without ILT for each patient. We observe that the concentration is nearly constant along the wall if ILT is not present. In the presence of ILT, the concentration significantly decreases (by roughly 50%)

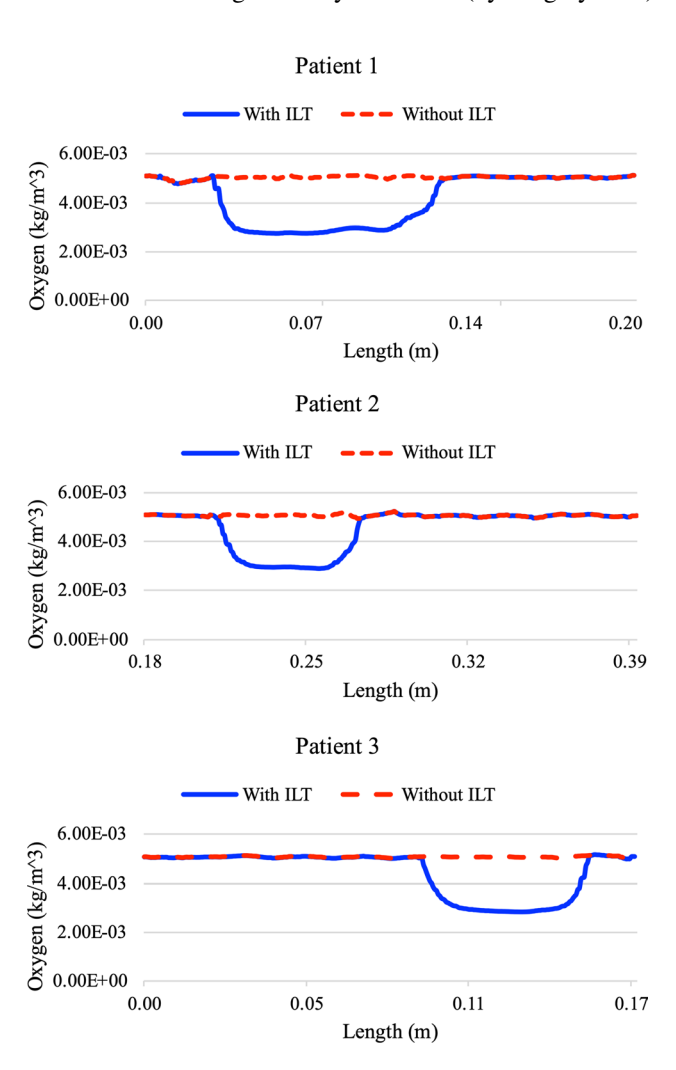


Fig. 8 Effect of ILT presence on oxygen concentration along the arterial wall in three AAA models



in the region between the ILT and AAA. In the case with the thickest ILT (patient 1), we observe a slightly larger reduction in the concentration compared to the other two patients.

The contours of oxygen diffusion flux on exterior surface of the aneurysmal wall, tunica adventitia layer, for three patient-specific AAA models are shown in Fig. 9. These plots qualitatively show that regions of low oxygen gradient along the AAA wall coincide with regions that experienced an ILT (top panel of Fig. 8), which indicates that hypoxia is closely related to the ILT presence. Comparison of oxygen gradient between the three AAA models with ILT and the same models when ILT is removed is observed. The simulations indicate that inclusion of the ILT influences the oxygen flow fields substantially. In particular, for the AAAs that include an ILT, the gradient plot indicates portions of low oxygen supply (hypoxic regions) at the blue colored sections of the bulge. Unlike the AAAs with the ILT, the AAAs that lack the ILT are in red color, represent significantly higher oxygen flow in the regions that previously were covered by ILT, and the distribution is more uniform across the wall region. Moreover, when ILT is removed, the contours of oxygen flux follow the same pattern for all the patients. Thus, there is no difference in oxygen gradient along the wall exterior for these cases. From the oxygen flux profiles on the tunica adventitia layer, we can clearly see that inclusion of an ILT causes a major reduction of the oxygen flow to the arterial wall in the regions neighboring the ILT. The presence of a larger and thicker ILT, i.e., in patient 1, causes a more noticeable decrease in oxygen flux to the outer surface of the aneurysmal wall. However, a patient with a small ILT has also lower oxygen flux within the wall compared with the same patient when ILT is excluded.

3.4 Model validation

Validation of the model is provided by comparing the results to existing literature. The obtained von Mises stress profiles on the arterial wall (Fig. 6) are compared with Bukac et al. (Bukač and Shadden 2021) that assesses the peak wall stress in the same patient-specific AAA models

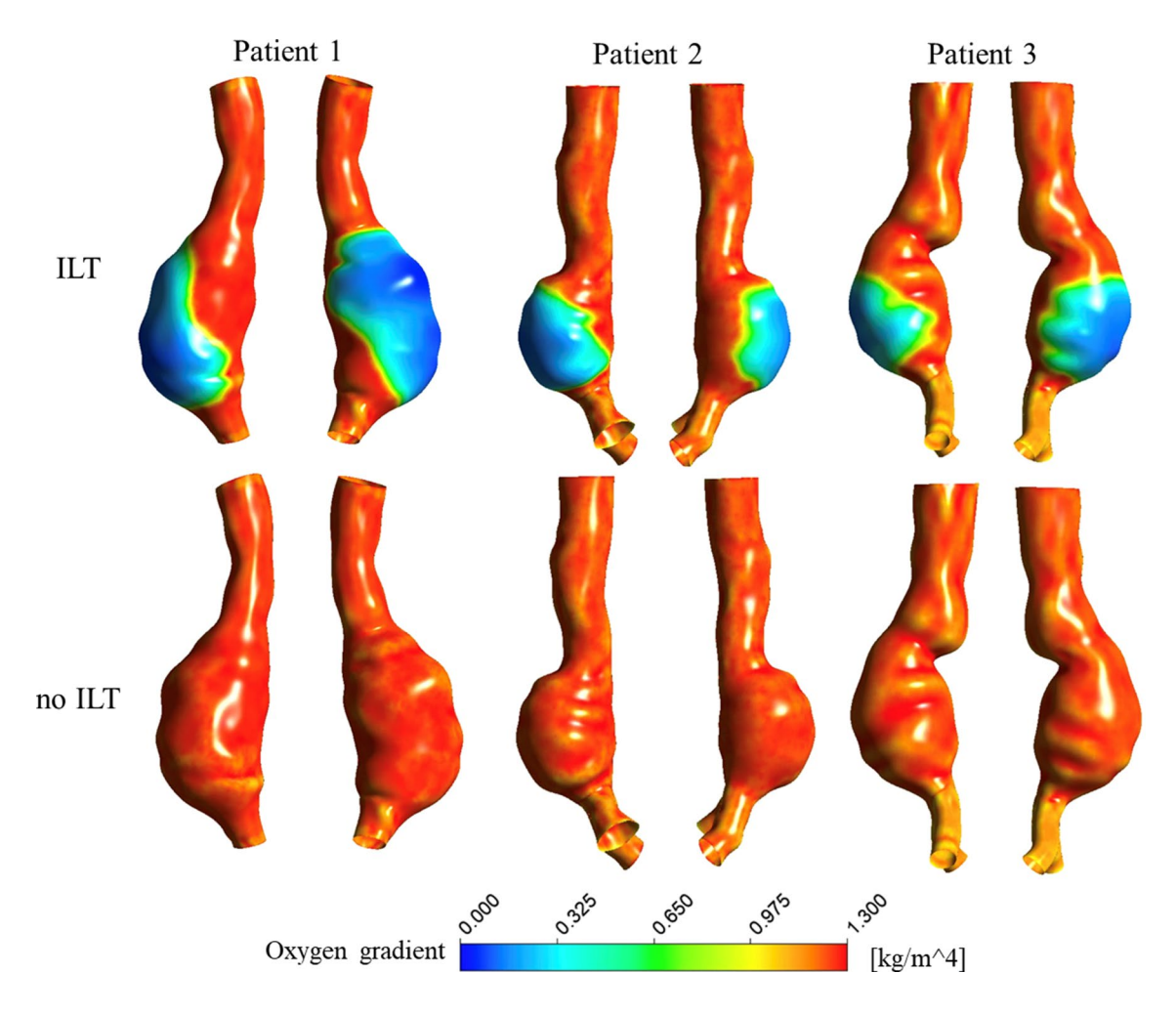


Fig. 9 Comparison of oxygen gradient distribution profiles on the tunica adventitia layer for different cases of AAA with an ILT (top row) and without an ILT (bottom row)



of this study by imposing a pulsatile velocity at the inlet of the fluid domain. The simulated peak von Mises wall stress for patient 1, patient 2, and patient 3 with an ILT is found to be 0.22 MPa, 0.28 MPa, and 0.24 MPa, respectively. The result for maximum von Mises stress provided in Table 4 shows good agreement with these values. We also found that the corresponding stress measurements for the three AAA patients without an ILT show agreement with results in Bukač and Shadden (2021). This is also consistent with calculated wall stresses of infrarenal aneurysmal wall by Li et al. (Li et al. 2008b), where the maximum von Mises stress was around 0.20 MPa in the presence of the ILT, and this value increased by 24% without the ILT. Moreover, in another related study, Wang et al. (Wang et al. 2002) observed that the wall principal stress was increased with the removal of the ILT, when systolic blood pressure was applied to the luminal surface. The obtained peak value was in the order of 0.40 MPa without the ILT but reduced to around 0.30 MPa with the ILT. Visual inspections also revealed a marked effect of ILT on the wall stress distribution. Finally, in a study by Riveros et al. (Riveros et al. 2015) the maximum wall stress was found to be 0.41 MPa. These observations for stress distribution correlate to the results of our study, both qualitatively and quantitatively. This indication is reinforced by several numerical studies that have demonstrated that ILT reduces wall stresses, by reducing the pressure load on the aneurysmal aortic wall.

The oxygen transport model is validated in Zakerzadeh et al. (Zakerzadeh et al. 2021) using idealized AAA geometries, and the obtained oxygen concentration profiles reported in the cited study were consistent with Vorp et al. (Vorp et al. 1998). More precisely, in Vorp et al. (Vorp et al. 1998), oxygen transport in four different idealized geometries of AAA using a simplified model that ignores blood flow inside the lumen has been studied, and we performed our simulation using similar idealized geometries. The obtained oxygen concentration profiles tested against Vorp et al.'s data, and the qualitative nature of the oxygen concentration is in agreement. We also compared the results of wall oxygen concentration obtained from in situ mass transport with experimental data for hypoxia in Vorp et al. (2001), where normalized partial pressure of oxygen in the ILT-wall interface, as well as a random point inside the AAA wall, for a large group of patients with thin and thick ILT has been reported, and hypoxia is defined as when the partial pressure of oxygen in the wall is less than 20% of its concentration inside the lumen. We have observed a qualitative agreement with these experimental results. However, it would be extremely difficult to find suitable clinical or in vitro data for quantitative validation since precise details such as variation in wall thickness, ILT thickness, and presence of vasa vasorum can significantly affect the results.

4 Conclusions and future work

4.1 Summary of the results

The role of the ILT in AAA mechanics remains controversial in the literature. Some studies concluded that the ILT has a protective role by reducing the wall stress, while others observed that AAAs with an ILT were at a greater risk of rupture despite the lower subsequent wall stress. One possible explanation of these conflicting observations is that there are two major factors involved in AAA rupture: the stress in the wall and the strength of the wall. AAA will rupture only when the local stress exceeds the local strength of the wall. Although our models suggest that ILT acts to reduce peak wall stress, this does not necessarily mean a lower risk of AAA rupture due to hypoxic wall weakening. The AAA wall strength may also be altered by the presence of ILT. Indeed, previous investigations by our group showed that presence of ILT is related to localized hypoxia (Zakerzadeh et al. 2021; Carbino et al. 2022) and therefore possibly wall weakening.

In this paper, we have developed a computational framework that provides the prediction of oxygen concentration in the arterial wall, as well as aortic wall stresses and deformation patterns, to compare the influence of the ILT on AAA hypoxia and rupture. Using this computational tool, we have explored a hypothetical clinical scenario, i.e., the inclusion or exclusion of the ILT, in three patient-specific AAA geometries by demonstrating the role of the altered flow dynamics due to the presence of ILT, and its effect on the arterial wall stresses distribution as well as oxygen transported to the aneurysmal wall. To our knowledge, this is the first study to evaluate the effect of ILT on both oxygen flow and wall stress in actual 3D reconstructed AAA. Using this combined model, our goal for this research is to explore the controversy for the role of the ILT in AAA mechanics.

The hemodynamic patterns in the lumen visualized using the velocity streamlines are shown in Fig. 3. In all cases regardless of the ILT presence, complex flow trajectories within the AAA lumen, specially at the bulge area, are found. At this portion of the AAA, the diameter is enlarged. The velocity accelerates at the outlets where the AAA diameter significantly decreases. The results indicate that the difference between the maximum pressure and minimum pressure is insignificant. Moreover, cases with ILT included have significantly different hemodynamic patterns, particularly flow recirculation regions, compared to cases where ILT was removed. It is also clear that intra aneurysmal flow is a function of geometric parameters of aneurysm and ILT, which is evident in the differing flow patterns among three patients.

Results are also presented for wall stress and deformation patterns and equivalent stress evolution. Namely, the



maximum principal stress and von Mises stress within the aneurysmal region, in the studied cases with and without ILT, are compared. As previously illustrated by the generated plots (Figs. 5 and 6), the resulting magnitude and location of the peak wall stresses is dependent on the shape of the AAA, and the ILT appears to reduce wall stresses for all patients.

The presence of the ILT seems to be a stabilizing factor for the AAA in terms of flow and stress distribution. A well-orientated ILT, which generates a channel like geometry with streamlined flow patterns, appears to reduce the stress and deformation in the AAA wall significantly. Stress variation can possibly alter the mechanical properties of the arterial wall, thus increasing AAA growth rate and risk of rupture. It was found that ILT has a significant effect on the wall stress magnitude and distribution, whereas there is a close relation between the ILT size and average oxygen concentration over the aneurysmal wall in AAAs. Patients without ILT had peak wall stress values which are significantly lower than patients with an ILT. It should be emphasized, however, that the stress levels are highly dependent on the geometry of the AAA and thus are patient specific. The results also indicate that the addition of the ILT decreases the concentration of oxygen along the wall, and ILT presence influences the oxygen flow fields substantially. This reduction in oxygen flow is more evident in patient 1 that contains a thicker and longer ILT. Patient 2 and patient 3 have ILTs that are comparable in thickness and volume, with ILT being to some degree larger for the second AAA, and therefore the oxygen concentration over wall is reduced slightly more in this case with respect to patient 3 (see Table 4).

Comparing the size of the analyzed aneurysms and ILTs (Table 1) with the results of peak values for stress and average oxygen concentrations within the AAA tissue (Table 4), it is clear that the geometrical features remain an important parameter in biomechanics of the AAA lesion. Moreover, we evaluated the percentages of change in stress measures and oxygen measure values in three patient-specific geometries with inclusion and exclusion of ILT from the simulation, to demonstrate how strongly removing ILT affects the model measures and which factor seems more dominant (see Table 4). On the basis of three representative aneurysms studied, the degree and significance of ILT presence on altering wall stress and oxygen measure depends on the unique ILT within each AAA.

Using the percentage of differences provided in Table 4, we conclude that the presence of ILT is correlated with reduced stress values and can enhance aortic wall strength; however, it also inhibits oxygen transport, namely the arterial wall is associated with lower average of oxygen concentrations. While a decrease in stress reduces the risk of rupture, increased local hypoxia could negatively impact AAA mechanics. Therefore, the protective biomechanical

advantage of ILT by lowering the wall stress may be outweighed by weakening of the AAA wall due to hypoxia. However, a larger study is needed to verify this hypothesis, which will be the focus of our future work.

In summary, our study indicates that the peak wall stresses and oxygen distributions are influenced by the presence of the ILT. For all the patients, the presence of the ILT decreases the wall deformation, reduces the AAA wall strength as a result of hypoxia, and decreases oxygen flow as well as the concentration of oxygen along the wall that increases the hypoxia. Therefore, while we found that ILT reduces the AAA wall stress, it also limits oxygen transport to the AAA wall, which may cause AAA wall degeneration. A biomechanical approach for AAA rupture risk assessment should account for the dynamic interaction of the intraluminal flow dynamics and the aortic wall as well as oxygen flow in patient-specific models. The relationship between ILT size and dynamic behavior of an AAA can be helpful in designing a patient-specific treatment. In this view, numerical simulations of the wall stress distribution and oxygen concentrations in AAAs by our coupled fluid-structure-mass transport approach could provide the additional and useful information for predicting AAA rupture risk. Accordingly, the inclusion of ILT in stress analysis of AAA is of importance and would likely increase the accuracy of predicting AAA rupture risk.

4.2 Limitations and future directions

Like most studies attempting to simulate an in vivo pathological condition, this investigation has limitations that need to be considered while interpreting the results. Although the analysis is of patient-specific AAA, the inlet velocity for each patient was not available. Instead, the results for hemodynamic simulations of this study are obtained based on typical values of pressure and volumetric flow rate of a healthy aorta for the inflow and outflow boundary conditions, for all patients. Although these assumed peak pressure and volumetric flow rate values are commonly used for setting up the boundary conditions, quantitative measurements of flow rates for individual patients will be needed for better estimation of the blood flow and resulting wall deformation. Despite the limitations that this assumption could have imposed, results in this study are consistent with previous findings as explained in Sect. 3.4 and we believe qualitatively the significance is low. While patient-specific velocity would have a certain effect on the results, for a parametric and comparative study such as presented here, keeping the same boundary conditions for both patients appear to be a valid assumption.

FSI simulations are done under steady-state flow. The assumption of steady-state FSI simulations has been analyzed previously in Sharzehee et al. (2018) and (Scotti, et al.



2008) for aneurysms and it has been observed that although pulsatile flow can give good approximation of stress field throughout the cardiac cycle, the difference of maximum aneurysm wall stress at pulsatile FSI flow and static pressure was 0% when non-uniform static pressure is used (Scotti, et al. 2008), as we have considered in luminal surface to deform our wall models. In another study (Geers et al. 2010), results for steady-state simulations and transient simulations for two intracranial aneurysms are compared. The effect of a change in maximum wall stress was investigated, and it was found that the difference in the wall stress on the aneurysm was less than 5% and the distribution of wall stress was qualitatively assessed to be very similar (Geers et al. 2010).

Therefore, we believe that the steady-state simulation used here does mimic the accurate representation of oxygen flow and stress measures from the dynamic application of intraluminal pressure and resulting wall deformation and stress distribution during the cardiac cycle in vivo. Ideally, a model for AAA wall stress distribution would use a dynamic pressure loading condition. However, this would result in greatly increased mathematic complexity, in particular for the oxygen transport model, and increased computational demands yet would not alter our current conclusions. For the purposes of comparison of wall stress distribution in AAA models with and without ILT, the worst-case scenario, or maximal stress distribution in the wall, is of more relevance than the actual temporal variation of the stress. Therefore. the steady-state simulations provide enough information for the purpose of this study at a lower computational cost, which could help facilitate the introduction of hemodynamic simulations into clinical practice.

The AAA wall and ILT are assumed to be homogeneous isotropic materials. Experimental evidence suggests that AAA wall is an anisotropic material, and ILT appears to be isotropic, although inhomogeneous, material. In addition, wall thickness is assumed uniform throughout the entire aneurysm due to the inherent limitations in the imaging technique and reconstruction. The degree of error introduced by these assumptions will be investigated in future studies. It should be noted that incorporation of these enhancements would not alter the conclusion that ILT alters the stress distribution and oxygen concentrations in AAA as the uniform thickness wall assumption is applied for both with- and without ILT cases in each patient and the value of the comparative results is still valid. Moreover, the residual stresses are not included in our model. Although the presence of longitudinal tension is likely to affect the wall stress in AAA, the purpose of this study is to investigate the effect of ILT on oxygen transport and wall stress distribution. Therefore, the resulting effect would be similar in both models with and without ILT, and our conclusion would remain valid. Finally, this study used sequential CT scans from three patients, and it would be ideal to increase the sample size to reach stronger conclusions. We note that removing the ILT regions from AAA models might result in a non-realistic flow geometry. However, comparing the computational results in AAAs with naturally present or absent ILTs in vivo would be difficult without a large-scale study due to many different features in patient-specific geometries which affect the model predictions. Although we obtained encouraging results, future work should comprise a larger population to take into account a wider range of possible geometries including aneurysms that are naturally without an ILT.

Acknowledgements We would like to thank Shawn Shadden and Miguel Rodriguez for providing us with the computational meshes. RZ is partially supported by the Samuel and Emma Winters Foundation and the NSF under grant CBET 2138225. MB is partially supported by the NSF under grants DMS 1912908 and DCSD 1934300.

Author contributions Conception and design: RZ and MB, Analysis and interpretation: RZ and AT, Data collection and visualization: AT, Writing the article: RZ, MB, and AT, Project administration and overall responsibility: RZ.

Declarations

Conflict of interest The authors declare that they have no conflict of interest.

References

Adolph R et al (1997) Cellular content and permeability of intraluminal thrombus in abdominal aortic aneurysm. J Vasc Surg 25(5):916–926

Swillens Al et al (2008) Effect of an abdominal aortic aneurysm on wave reflection in the Aorta. IEEE Trans Biomed Eng 55:1602–1611

Amanuma M et al (1992) Abdominal aorta: characterisation of blood flow and measurement of its regional distribution by cine magnetic resonance phase-shift velocity mapping. Eur Radiol 2(6):559–564

Ayyalasomayajula A, Vande Geest JP, Simon BR (2010) Porohyperelastic finite element modeling of abdominal aortic aneurysms. J Biomech Eng 132(10):104502

Bhagavan D, Di Achille P, Humphrey JD (2018) Strongly coupled morphological features of aortic aneurysms drive intraluminal thrombus. Sci Rep 8(1):13273

Bluestein D et al (2009) Intraluminal thrombus and risk of rupture in patient specific abdominal aortic aneurysm – FSI modelling. Comput Methods Biomech Biomed Engin 12(1):73–81

Boyd AJ (2021) Intraluminal thrombus: Innocent bystander or factor in abdominal aortic aneurysm pathogenesis? JVS: Vascular Science

Buerk DG, Goldstick TK (1982) Arterial wall oxygen consumption rate varies spatially. Am J Physiol-Heart and Circulatory Physiol 243(6):H948–H958

Buerk DG, Goldstick TK (1986) Oxygen tension changes in the outer vascular wall supplied by vasa vasorum following adenosine and epinephrine. J Vasc Res 23(1):9–21

Bukač M, Shadden SC (2021) Quantifying the effects of intraluminal thrombi and their poroelastic properties on abdominal aortic aneurysms. Archive of Appl Mech 92:435–446



- Caputo M et al (2013) Simulation of oxygen transfer in stented arteries and correlation with in-stent restenosis. Int J Numer Method Biomed Eng 29(12):1373–1387
- Carbino B et al (2022) The effects of geometric features of intraluminal thrombus on the vessel wall oxygen starvation. Manuscript Accepted for Publication in Front Bioeng Biotechnol. https://doi.org/10.3389/fbioe.2022.814995
- Cheng CP, Taylor CA, Dalman RL (2015) Abdominal aortic hemodynamics in intermittent claudication patients at rest and during dynamic pedaling exercise. Ann Vasc Surg 29(8):1516–1523
- Chimakurthi SK et al (2018) ANSYS workbench system coupling: a state-of-the-art computational framework for analyzing multiphysics problems. Eng Comput 34(2):385–411
- Chiu K et al (2014) Ultrasound measurement for abdominal aortic aneurysm screening: a direct comparison of the three leading methods. Eur J Vasc Endovasc Surg 47(4):367–373
- Coutard M et al (2010) Thrombus versus wall biological activities in experimental aortic aneurysms. J Vasc Res 47(4):355–366
- da Silva ES et al (2000) Morphology and diameter of infrarenal aortic aneurysms: a prospective autopsy study. Cardiovasc Surg 8(7):526–532
- Di Martino E et al (1998) Biomechanics of abdominal aortic aneurysm in the presence of endoluminal thrombus: experimental characterisation and structural static computational analysis. Eur J Vasc Endovasc Surg 15(4):290–299
- Douek PC (2005) Contrast-enhanced MR angiography of the abdominal Aorta. Magnetic resonance angiography. Springer, pp 195–208
- Fournier, R.L., Basic transport phenomena in biomedical engineering. 2017: CRC press.
- Geers AJ et al (2010) Comparison of steady-state and transient blood flow simulations of intracranial aneurysms. Annu Int Conf IEEE Eng Med Biol Soc 2010:2622–2625
- Geest JPV, Sacks MS, Vorp DA (2006) A planar biaxial constitutive relation for the luminal layer of intra-luminal thrombus in abdominal aortic aneurysms. J Biomech 39(13):2347–2354
- Georgakarakos E et al (2009) on abdominal aortic aneurysm wall stress. Int Angiol 28:325–333
- Geuzaine C, Remacle JF (2009) Gmsh: A 3-D finite element mesh generator with built-in pre-and post-processing facilities. Int J Numer Meth Eng 79(11):1309–1331
- Haller SJ et al (2018) Intraluminal thrombus is associated with early rupture of abdominal aortic aneurysm. J Vascular Surg 67(4):1051–1058
- Harter LP et al (1982) Ultrasonic evaluation of abdominal aortic thrombus. J Ultrasound Med 1(8):315–318
- Iannetti L et al (2016) Distributed and lumped parameter models for the characterization of high throughput bioreactors. PLoS ONE 11(9):e0162774
- Kazi M et al (2003) Influence of intraluminal thrombus on structural and cellular composition of abdominal aortic aneurysm wall. J Vasc Surg 38(6):1283–1292
- Kemmerling EMC, Peattie RA (2018) Abdominal aortic aneurysm pathomechanics: current understanding and future directions. Adv Exp Med Biol 1097:157–179
- Ku DN (1997) Blood flow in arteries. Annu Rev Fluid Mech 29(1):399-434
- Kühnl A et al (2017) Incidence, treatment and mortality in patients with abdominal aortic aneurysms: an analysis of hospital discharge data from 2005–2014. Dtsch Arztebl Int 114(22–23):391
- Li Z-Y et al (2008a) Impact of calcification and intraluminal thrombus on the computed wall stresses of abdominal aortic aneurysm. J Vasc Surg 47(5):928–935
- Lim CS et al (2013) Hypoxia-inducible factor pathway and diseases of the vascular wall. J Vasc Surg 58(1):219–230
- Moore J, Ethier C (1997) Oxygen mass transfer calculations in large arteries

- Mower WR, Quiñones WJ, Gambhir SS (1997) Effect of intraluminal thrombus on abdominal aortic aneurysm wall stress. J Vasc Surg 26(4):602–608
- Moxon JV et al (2010) Diagnosis and monitoring of abdominal aortic aneurysm: current status and future prospects. Curr Probl Cardiol 35(10):512–548
- Polzer S et al (2011) The impact of intraluminal thrombus failure on the mechanical stress in the wall of abdominal aortic aneurysms. Eur J Vasc Endovasc Surg 41(4):467–473
- Polzer S et al (2012) Impact of poroelasticity of intraluminal thrombus on wall stress of abdominal aortic aneurysms. Biomed Eng Online 11:62–62
- Polzer S, Bursa J (2010) Poroelastic model of intraluminal thrombus in FEA of aortic aneurysm. in 6th World Congress of Biomechanics (WCB 2010). August 1–6, 2010 *Singapore*: Springer.
- Raghavan M, Vorp DA (2000) Toward a biomechanical tool to evaluate rupture potential of abdominal aortic aneurysm: identification of a finite strain constitutive model and evaluation of its applicability. J Biomech 33(4):475–482
- Rappitsch G, Perktold K (1996) Computer simulation of convective diffusion processes in large arteries. J Biomech 29(2):207–215
- Raptis A et al (2016) Effect of macroscale formation of intraluminal thrombus on blood flow in abdominal aortic aneurysms. Comput Methods Biomech Biomed Engin 19(1):84–92
- Reymond P et al (2009) Validation of a one-dimensional model of the systemic arterial tree. Am J Physiol-Heart and Circulatory Physiol 297(1):H208-H222
- Riveros F et al (2015) On the impact of intraluminal thrombus mechanical behavior in AAA passive mechanics. Ann Biomed Eng 43(9):2253–2264
- Scotti CM et al (2008) Wall stress and flow dynamics in abdominal aortic aneurysms: finite element analysis vs fluid-structure interaction. Comput Methods Biomech Biomed Engin 11(3):301–22
- Sharzehee M, Khalafvand SS, Han HC (2018) Fluid-structure interaction modeling of aneurysmal arteries under steady-state and pulsatile blood flow: a stability analysis. Comput Methods Biomech Biomed Engin 21(3):219–231
- Shin I-S et al (2009) Early growth response factor-1 is associated with intraluminal thrombus formation in human abdominal aortic aneurysm. J Am Coll Cardiol 53(9):792–799
- Stergiou Y et al (2019) Fluid-structure interaction in abdominal aortic aneurysms: effect of haematocrit. Fluids 4(1):11
- Sun N et al (2009) Computational analysis of oxygen transport in a patient-specific model of abdominal aortic aneurysm with intraluminal thrombus. Br J Radiol 82:18–23
- Updegrove A et al (2017) SimVascular: an open source pipeline for cardiovascular simulation. Ann Biomed Eng 45(3):525–541
- Virag L et al (2015) A computational model of biochemomechanical effects of intraluminal thrombus on the enlargement of abdominal aortic aneurysms. Ann Biomed Eng 43(12):2852–2867
- Vorp D et al (1996a) Potential influence of intraluminal thrombus on abdominal aortic aneurysm as assessed by a new non-invasive method. Cardiovasc Surg 4(6):732–739
- Vorp D et al (1998) Effect of intraluminal thrombus thickness and bulge diameter on the oxygen diffusion in abdominal aortic aneurysm. J Biomech Eng 120(5):579–583
- Vorp DA et al (2001) Association of intraluminal thrombus in abdominal aortic aneurysm with local hypoxia and wall weakening. J Vasc Surg 34(2):291–299
- Vorp DA, Federspiel WJ, Webster MW (1996b) Does laminated intraluminal thrombus within abdominal aortic aneurysm cause anoxia of the aortic wall? J Vasc Surg 23(3):540–541
- VosseStergiopulos FNvdN (2011) Pulse wave propagation in the arterial tree. Annual Rev Fluid Mech 43(1):467–499



- Wang DH et al (2002) Effect of intraluminal thrombus on wall stress in patient-specific models of abdominal aortic aneurysm. J Vasc Surg 36(3):598–604
- Wilson JS et al (2013) Biochemomechanics of intraluminal thrombus in abdominal aortic aneurysms. J Biomech Eng 135(2):021011
- Zakerzadeh R et al (2021) Coupled hemodynamics and oxygen diffusion in abdominal aortic aneurysm: a computational sensitivity study. Cardiovasc Eng Technol 12(2):166–182
- Zakerzadeh R, Cupac T, Durka M (2020) Oxygen transport in a permeable model of abdominal aortic aneurysm. Comput Methods in Biomech Biomed Eng 24:215–229
- Zambrano BA et al (2016) Association of intraluminal thrombus, hemodynamic forces, and abdominal aortic aneurysm expansion using longitudinal CT images. Ann Biomed Eng 44(5):1502–1514

Publisher's Note Springer Nature remains neutral with regard to jurisdictional claims in published maps and institutional affiliations.

Springer Nature or its licensor holds exclusive rights to this article under a publishing agreement with the author(s) or other rightsholder(s); author self-archiving of the accepted manuscript version of this article is solely governed by the terms of such publishing agreement and applicable law.

